Journal of the Korean Physical Society, Vol. 49, December 2006, pp. S314∼S319

Launcher Study for KSTAR 5 GHz LHCD System

Young S. BAE*
KSTAR Operation Division, National Fusion Research Center, Daejeon 305-333

Moo H. CHO and Won NAMKUNG
Department of Physics, Pohang University of Science and Technology, Pohang 790-784

S. BERNABEI, R. ELLIS, J. WILSON, J. HOSEA and H. PARK
Princeton Plasma Physics Laboratory, Princeton, NJ 08543, U.S.A

(Received 29 August 2005)

A 5 GHz Lower Hybrid Current Drive (LHCD) system with 2 MW is under development for the steady-state operations of the KSTAR. The present design of fully active waveguide launcher gives very good spectral directivity of more than 90 % for the phase shift of 90 degrees and a wider $N_\parallel$ range of 1.4 to 3.6 with a width $\Delta N_\parallel = 0.54$. For the steady-state operations of the KSTAR, a Glidcop/SS sandwiched grill is proposed with consideration of heat and disruption loads. A PAM (Passive-Active Multi-junction)-type launcher is also studied for the possibility of use for the KSTAR. The PAM-type launcher provided good coupling properties even at lower edge densities in FTU 8 GHz PAM launcher tests. However, it gives a lower current drive efficiency compared with the conventional grill because of reduced directivities. The Passive/Active grill has 30 % less directivity than the Fully Active grill from the characteristic studies on the directivity and coupling. On the other hand, it gives a good coupling property with weak dependence on the phase shift between adjacent waveguides.

PACS numbers: 52.50.G, 52.55
Keywords: KSTAR, Lower-hybrd, Launcher

I. INTRODUCTION

The recent interest in the LHCD system is mainly to control and to shape the plasma current profiles rather than the plasma heating [1–3]. The off-axis current driven by the LH waves can create broad or even hollow current profiles required in the 'advanced tokamak' scenario for ITER by introducing a negative shear [4]. Therefore, the LH system is expected to provide a major contribution to the advanced tokamak experiments in the steady-state KSTAR operations (300 s). The KSTAR 5 GHz, 2 MW CW LHCD system is under development. The RF frequency of LH wave is chosen as 5 GHz for the KSTAR, which is the same as the ITER LH frequency. For 5 GHz RF source, an order for a prototype of 5 GHz, 500 kW CW klystron is placed with Toshiba Electron Tubes & Devices (TETD) Co., and it is under fabrication. Phased waveguide arrays are generally being used for launching LH waves in a tokamak. The concept of the conventional 'grill' [5] - an array of independent waveguides - is used to design the KSTAR LH launcher. In recent years, the basic design on the 5 GHz LH launcher with fully active waveguide channels has been carried out in collaboration with PPPL [6,7]. The design has many features which are the same as in the C-MOD LHCD system, which will serve to test these features for relatively short pulses of 5 s. The near steady state of the KSTAR operation, however, requires somewhat new challenges for heat removal in the grill and for compact waterloads absorbing the reflected RF power. It also means that the ITER-relevant launcher based on the PAM (Passive Active Multi-junction) concept could be an alternative candidate for the KSTAR LH launcher because the PAM launcher was successfully validated in FTU [8]. The test of a PAM launcher on FTU shows the first step toward the LHCD launcher for ITER. In this paper, the present design of 5-GHz KSTAR LH launcher is described in Sections II and III. The PAM launcher test on FTU is introduced in Section IV. Also, the PAM concept on the KSTAR LH launcher is compared with the fully active launcher for power directivity and coupling, and conclusions are then given.

*E-mail: ysbae@nfrc.re.kr

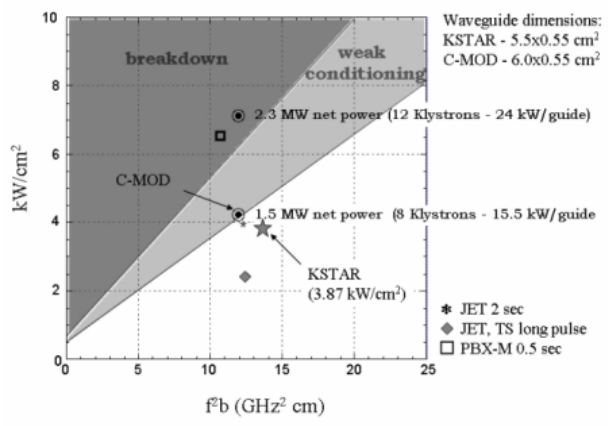

Fig. 1. Power flux density in C-MOD and KSTAR grill [7]

II. 5-GHZ KSTAR LH LAUNCHER

1. Power spectrum and coupling properties

The present design of 5 GHz KSTAR LH launcher has a very good spectral controllability by phasing of each waveguide column in the grill. The grill is composed of fully 32 active waveguide columns by 4 rows. Each waveguide width and height is 5.5 mm and 55.0 mm, respectively, and it is separated by a 1.5 mm thick septum. The waveguide size in the grill is compromised for the power flux density in the grill below a weak breakdown conditioning regime as shown in Fig. 1 as well as for a higher fundamental peak $N_{\|}$ (see Eq. (1)) than the accessible $N_{\|}$ given by the Golant condition (see Eq. (2)).

$$N_{||n} = \frac{\Delta\phi}{kp} + n\frac{\pi}{kp}, \tag{1}$$

$$\begin{aligned} N_{||,acc} &= \frac{\omega_{pe}}{\omega_{ce}} + \left[1 + \frac{\omega_{pe}^2}{\omega_{ce}^2} - \frac{\omega_{pi}^2}{\omega^2}\right]^{1/2} \\ &= 3.21\frac{\sqrt{n_e}}{B_T} + \left[1 + \frac{10.33}{B_T^2}n_e\left(1 - 0.427A\frac{B_T^2}{f_{LH}^2}\right)\right]^{1/2}, \end{aligned} \tag{2}$$

where k is the vacuum wavenumber, $\Delta\phi$ is the phase shift between adjacent waveguides, p is the geometric periodicity of waveguides, and n is an integer mode number. The position of the fundamental peak $N_{\|0}$ of the radiated spectrum is 2.13 for the KSTAR LH grill with p = 7 mm, $\Delta\phi = \pi/2$. Fig. 2 shows the radiated power spectra and the integrated coupling power efficiency over $N_{\|}$ for various phase shifts when using the Steven's code [9]. The accessible $N_{\|} = 2.0$ is given for $f_{LH} = 5$ GHz, $B_T = 3.5$ T, A is the atomic mass number of hydrogen, 1, $n_e = 1 \times 10^{20}\,\mathrm{m}^{-3}$, and $N_{\|acc} = 2.0$.

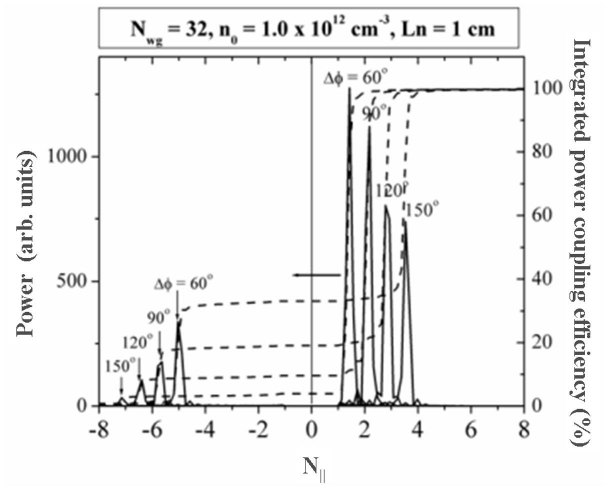

Fig. 2. Radiated power spectrum and integrated power coupling efficiency over $N_{\|}$ are given for their phase shifts of 60°, 90°, 120°, and 150° with edge density, $n_0 = 1 \times 10^{12}\,\mathrm{cm}^{-3}$, and density gradient, $\nabla n = n_0/L_n = 1 \times 10^{13}\,\mathrm{cm}^{-3}$

The power directivity, D_p, and the $N_{\|}$-weighted directivity, D_{cd}, which is defined with respect to the current drive efficiency, are given by

$$D_p = \int_1^\infty \frac{dP}{dN_{\|}}dN_{\|} / \int_{-\infty}^\infty \frac{dP}{dN_{\|}}dN_{\|}, \tag{3}$$

and

$$\begin{aligned} D_{cd} &= (1-R)N_{\|peak}^2 \\ &\times \left(\int_1^\infty \frac{1}{N_{\|}^2}\frac{dP}{dN_{\|}}dN_{\|} - \int_{-\infty}^{-1} \frac{1}{N_{\|}^2}\frac{dP}{dN_{\|}}dN_{\|}\right), \end{aligned} \tag{4}$$

respectively. From the vertical axis of the right hand side in Fig. 2, the power directivities are easily obtained as 96 %, 91 %, 81 %, and 67 % for each phase shift of 60°, 90°, 120°, and 150°, but the definition of D_{cd} gives $N_{\|}$-weighted directivities of 93 %, 89 %, 72 %, and 45 %. Fig. 3 shows the directivities as a function of the grill edge plasma density. The maximum value of $N_{\|}$-weighted directivities corresponds to the minimum reflection at the same edge density.

The optimum coupling edge density at the grill is calculated by using the linear coupling theory in two regimes: a) the "cutoff regime" at a lower density, and b) the "WKB regime" at a moderate density without taking into consideration the high density effect where $E \times B$ current cannot be neglected [10]. The density gradient is a key parameter in the cutoff regime at low edge density, and the edge density is a key parameter in the "WKB regime" at moderate density. For the "WKB regime", the optimum edge density ratio to the cutoff density is

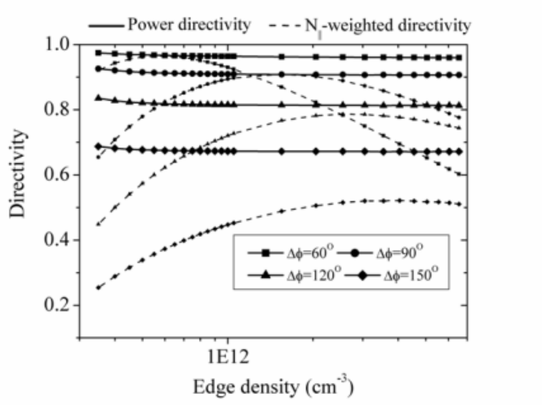

Fig. 3. Two different directivities as a function of grill edge plasma density.

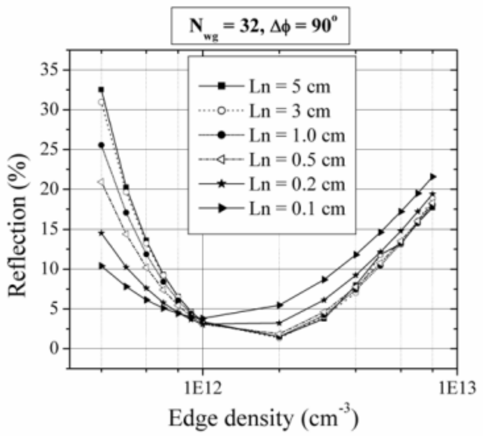

Fig. 4. Reflection from the grill edge as a function of edge density for various scale lengths of the density gradient.

theoretically given by [9].

$$\frac{n_0}{n_c} = N_{\parallel}^2(1 - (\frac{\pi}{k_0 h})) + (\frac{pi}{k_0 h})^2 \tag{5}$$

where n_0 is the edge density at grill, n_c is the cutoff density where the plasma frequency is the same as the LH wave frequency ($n_c = 3 \times 10^{11}\,\mathrm{cm}^{-3}$ for 5 GHz), and h is the waveguide height. For KSTAR, $n_0/n_c = 3.54$ for $\Delta\phi = \pi/2$ (peak $N_{\parallel} = 2.15$). Fig. 4 shows the results by the Steven's code on the coupling effects of the fully active grill for the KSTAR on low-edge-density and moderate-density regimes by using step and linear density ramping in front of the grill.

This shows that the best coupling edge density is about 3.3 $n_c \sim 1 \times 10^{12}\,\mathrm{cm}^{-3}$ for scale length less than 0.2 cm. One may note that the coupling has less density-gradient dependency for edge density higher than $8 \times 10^{11}\,\mathrm{cm}^{-3}$. The best coupling with the minimum reflection, which is less than 2 %, is obtained with edge density around $2 \times 10^{12}\,\mathrm{cm}^{-3}$, but this is not in accord with results from numerical calculation of non-linear coupling and particle simulation [11,12].

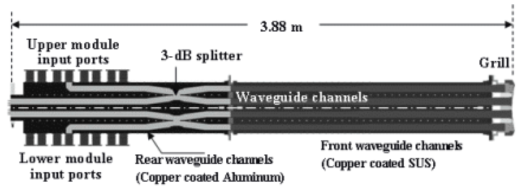

Fig. 5. Cross section drawing of waveguide channel.

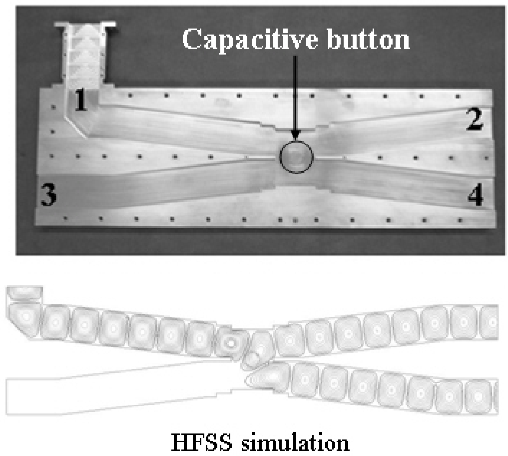

Fig. 6. (Upper) Test module of 3-dB power splitter, and (lower) electric field contour plot in HFSS simulation.

2. Waveguide channel design

The KSTAR LH launcher is composed of 64 waveguide channels, 32 channels each for the upper and lower modules, patterned on the metal plate. The grill is attached to the end of the waveguide channels. The channels are stacked with bolts through the metal plates. The waveguide pattern in each channel is shown in Fig. 5.

The key pattern is the 3-dB power splitter for even power splitting into the vertical output waveguides. The optimized design of the 3-dB power splitter is obtained by introducing a capacitive button at the center of the 3-dB power splitter. This is just an extrusion of metal cylinder with a height of 1.3 mm. Fig. 6 shows the test module of the 3-dB power splitter with a capacitive button and HFSS simulation results. From the low-power test of the test module, the same output power of −3.43 dB at each output waveguide is obtained, and the return loss (S11) and the isolation to the matched waveguide (S31) are all less than −30 dB.

III. STEADY-STATE DESIGN ISSUES FOR THE KSTAR LH LAUNCHER

The present design of the KSTAR LH launcher has many features as for the C-MOD LH launcher. How-

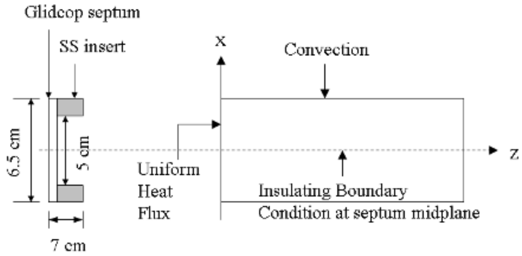

Fig. 7. Schematic of 3-dimensional ANSYS finite-element model for the stacked construction with Glidcop septum and cooled SS insert.

ever, the long pulse (300 s) operation of the KSTAR requires some new design considerations for the KSTAR LH launcher. The requirements and challenges for the new launcher features are: better heat removal from the grill nose, shielding of the microwave windows from direct line of sight to the plasma, and compact water loads for capturing and absorbing power reflected from the grill edge plasma. The heat removal from the grill nose is the major critical issue for steady-state operation. Two possible solutions for KSTAR LH launcher cooling could be as follows;

1. Incorporate Frascati ITER PAM grill type; it is good for the good cooling but reduces active guides by half and reduces directivity of the radiated power spectrum.

2. Design the cooling into the present stacked metal plate of the KSTAR launcher design; it keeps the optimum spectral control but the 1.5 mm stainless steel septum could not provide the heat conductivity.

For the second solution, the material must be changed to Glidcop or CuCrZr or cooling tubes embedded into septum. A proper design of Glidcop/SS sandwiched grill, that is, a stacked construction with Glidcop septum and water cooled stainless steel insert as seen in Fig. 7, is obtained using the ANSYS program [13] in collaboration with PPPL. The ANSYS finite-element model of Glidcop/SS sandwiched grill as shown in Fig. 7, using SOLID90 thermal elements and SURF152 elements to specify radiation and heat convection boundary conditions, was constructed for the configurations to be studied.

In this model, the x, y, and z coordinates correspond to the vertical, toroidal, and outward radial directions. For simplicity, only half the waveguide is used when using the insulating boundary condition on septum midplane. The uniform heat flux from the plasma is assumed to be 100 W/cm^2. The convection film coefficient for the top of the grill water cooled within 5 mm from the front edge is set to 1.6 W/cm^2 K with a water coolant bulk temperature of 20 °C. The thermal conductivities for the

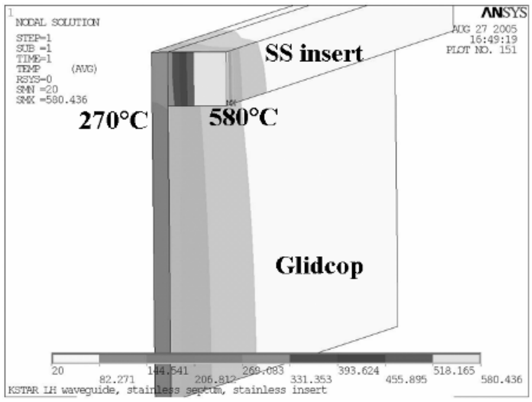

Fig. 8. Temperature distribution results from ANSYS simulation.

Glidcop septum and SS insert are given as a function of temperature:

$$k_{Glidcop} = 3.65 - 0.00052\,T\,[\mathrm{W/cm^2 \cdot K}],$$
$$k_{SS} = 0.163 + 0.000147\,T\,[\mathrm{W/cm^2 \cdot K}]. \quad (6)$$

Fig. 8 shows the ANSYS analysis results. The maximum temperature of 580 °C is seen in the front edge of SS insert, and therefore this design would give the adequate performance for steady -state operation on the KSTAR.

IV. CHARACTERISTICS OF PAM LAUNCHER AND BASIC STUDIES ON PASSIVE/ACTIVE GRILL FOR KSTAR

In this section, the concept of PAM (Passive-Active Multi-junction) launcher and FTU PAM launcher test results are introduced. Also, the basic characteristics of the Passive-Active grill with the passive waveguide 90° phased are compared with those of the fully active grill.

The necessity for the passive waveguide originats from minimizing the surface-wave component of the radiated power because surface waves give rise to undesirable nonlinear interactions [14–17]. Surface wave can be minimized by employing multiple waveguide arrays as well as by driving the outside guides at a reduced power [18]. It was observed that there was a reduction in the width of the resonance cone and in the amplitude of the surface wave component by a factor of ∼3 when the passive waveguides (tuners or dummy guides) were added in each side of the twin guide array [19]. The detailed results of LHCD and coupling experiments with the ITER-like PAM launcher at 8 GHz at FTU are found in Ref. [8]. Fig. 9 shows the ITER-like PAM launcher used at FTU. The maximum achieved value of the routine power density was 80 MW/m^2, that would be only 52 MW/m^2 by scaling with the frequency. This is at least 1.4 times larger than the ITER request of 33 MW/m^2 required for

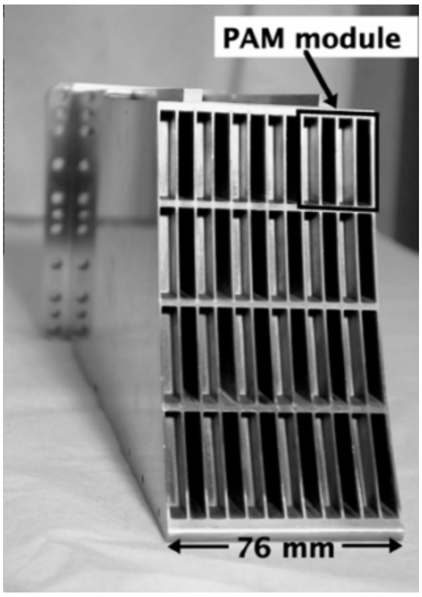

Fig. 9. FTU PAM launcher [8].

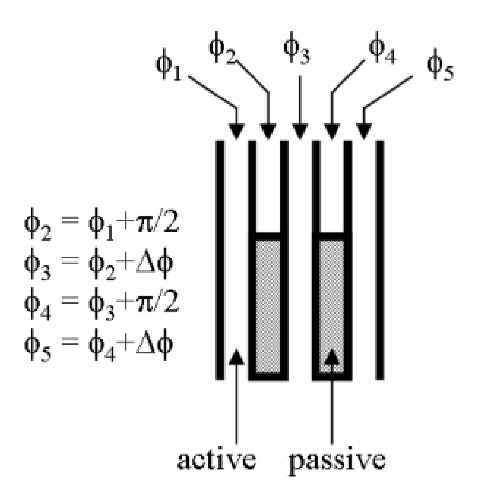

Fig. 10. Simple Passive-Active grill structure.

the ITER grill in order to couple 20 MW to the plasma. Also, they obtained very good coupling throughout the SOL plasma, provided the antenna is properly conditioned to avoid gas release from the internal waveguide walls. The average reflection coefficient ρ_c is $\approx$1.3 %, and never exceeded 2.5 %, even with almost evanescent plasmas in front of the grill, as when this was fully retracted inside the port (up to 3 mm) to simulate the ITER operation, and the density at its mouth was equal to or even lower than the cut-off value, but, on current drive (CD) efficiency, PAM CD is lower. However authors in Ref. [8] conclude that it is not degraded with respect to a conventional grill launching a similar $N_{\|}$ spectrum, taking into account the lower power directivity. The basic study on directivity and coupling characteristics of Passive-Active grill and Fully Active grill is

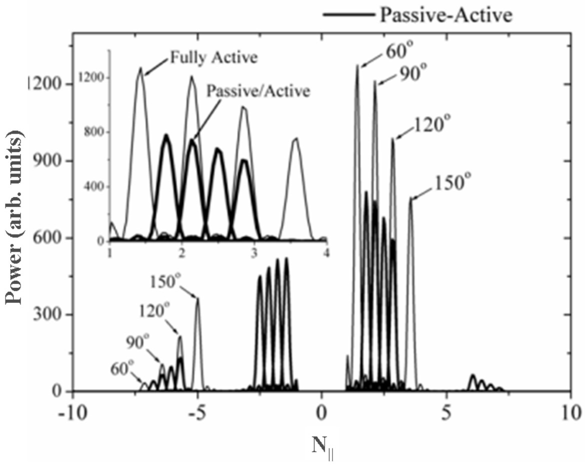

Fig. 11. Radiated power spectrum in passive-active grill and fully active grill for the phase shifts.

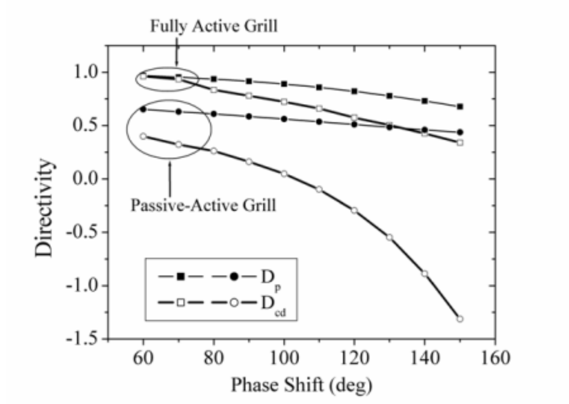

Fig. 12. Directivities as a function of phase shift for passive-active grill and fully active grill.

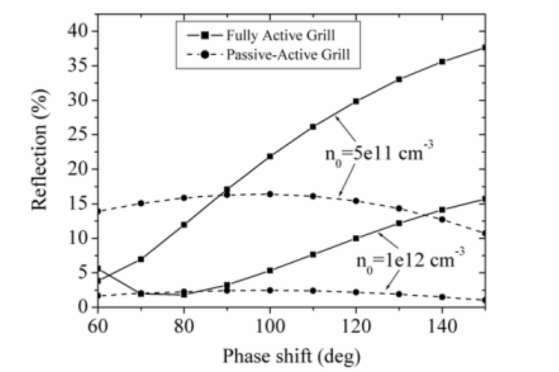

Fig. 13. Reflection as a function of phase shift for passive-active grill and fully active grill.

carried out by using the Steven's code as well. For the Passive/Active grill, the simple model is shown in Fig. 10. It is assumed that every other passive waveguide is 90°-phased and 1-% field-power crossed to the adjacent active waveguides in the calculation. Note that only the first pass before the reflection back from the short plane of the passive waveguide and no multi-junction type are considered.

Fig. 11 shows the radiated power spectrum from the fully active grill and the simple passive-active grill. The passive-active grill has many other peaks not having negligible power.

In Fig. 12, directivity and coupling are compared as a function of the phase shift between adjacent waveguides. The fully active grill gives much better directivity and wider $N_{\|}$ range compared with the passive-active grill. The passive-active grill has opposite $N_{\|}$-weighted directivity as the phase shift increases, but, for the coupling in the "WKB regime" of the edge density, the passive-active grill gives better coupling in a wide range of phase shifts, as shown in Fig. 13.

V. CONCLUSION

The fully active waveguides for the 5-GHz KSTAR LH launcher give a very good spectral directivity and a wider $N_{\|}$-range. The important issues for the steady-state KSTAR LH launcher are designing, analyzing, and high-power prototype of fully active grills that can sustain steady-state operations in the KSTAR. A Glidcop/SS sandwich would be best for heat and disruption loads although detailed stress analysis is necessary in order to validate this design for the disruption load. Good metallic bonding between Glidcop and stainless steel could be possible if Ni-coated Glidcop were brazed with stainless steel. Further physical and mechanical engineering studies on this design will be continued in the near future. The other issues are the proper placement of windows out-of-sight of plasma and the design of the compact water load for the matched waveguide (arm 3) of the 3-dB power splitter and its prototype at low and high power levels. The PAM launcher proves to have good coupling properties, even at a lower edge density, in FTU 8 GHz PAM launcher tests. However, it gives a lower current drive efficiency compared with the conventional grill because of reduced directivity. From the directivity and coupling studies for the Passive/Active grill and the Fully Active grill for the KSTAR, the Passive/Active grill has 30 % reduced directivity, but it gives a good coupling property with weak dependence on the phase shift between adjacent waveguides. If lower $N_{\|}$ proves to be optimum for the KSTAR, the PAM design could be an alternative for the KSTAR. In addition, it proves to be acceptable for the ITER.

ACKNOWLEDGMENTS

This work was supported by the KSTAR Project, NFRC.

REFERENCES

[1] X. Litaudon, R. Arslanbekov, G. T. Hoang, E. Joffrin, F. Kazarian-Vibert, D. Moreau, Y. Peysson, P. Bibet, P. Froissard, M. Goniche, G. Rey, J. Ferron and K Kupfer, Plasma Phys. Controlled Fusion **38**, 1603 (1996).
[2] S. H. Kim, J. M. Park and S. H. Hong, J. Korean Phys. Soc. **46**, 861 (2005).
[3] B. G. Hong, J. Korean Phys. Soc. **36**, 90 (2000).
[4] J. Mailloux, B. Alper, Y. Baranov, A. Becoulet, A. Cardinali, C. Castaldo, R. Cesario, G. Conway, C. D. Challis, F. Crisanti, M. de Baar, P. de Vries, A. Ekedahl, K. Erents, C. Gowers, N. C. Hawkes, G. M. D. Hogeweij, F. Imbeaux, E. Joffrin, X. Litaudon, P. Lomas, G. F. Matthews, D. Mazon, V. Pericoli, R. Prentice, F. Rimini, Y. Sarazin, B. C. Stratton, A. A. Tuccillo, T. Tala and K.-D. Zastrow, Phys. Plasma **9**, 2156 (2002).
[5] M. Brambilla, Nucl. Fusion **16**, 47 (1976).
[6] Y. S. Bae, C. H. Paek, M. J. Rhee, W. Namkung, M. H. Cho, S. Bernabei and H. Park, Fusion Eng. Design **65**, 569 (2003).
[7] J. Hosea, S. Bernabei, R. Ellis and J. R. Wilson, *US-Korea Workshop* (General Atomic, 2004).
[8] V. Pericoli Ridolfini, Ph. Bibet, F. Mirizzi, M. L. Apicella, E. Barbato, P. Buratti, G. Calabrò, A. Cardinali, G. Granucci, L. Panaccione, S. Podda, C. Sozzi and A. A. Tuccillo, Nucl. Fusion **45**, 1085 (2005).
[9] J. Stevens, M. Ono, R. Horton and J. R. Wilson, Nucl. Fusion **21**, 1259 (1981).
[10] D. Moreau, C. Gormezano, G. Melin and T. K. Nguyen, in *Proceedings ot the Spring College Trieste)(1983)*, (World Scientific, Singapore, 1984), p. 331.
[11] Y. S. Bae, M. H. Cho and W. Namkung, J. Korean Phys. Soc. **44**, 1207 (2004).
[12] Y. S. Bae, W. Namkung and M. H. Cho, *9th Asia Pacific Physics Conference* (Hanoi, 2004).
[13] 3D Structural, Thermal, EM analysis software using Finite Element Method, Ansys Inc., http://www.ansys.com/.
[14] G. J. Morales, Phys. Fluids **20**, 1164 (1977).
[15] M. Porkolab and R. P. H. Chang, Rev. Mod. Phys. **50**, 745 (1978).
[16] R. W. Motley, W. M. Hooke and G. Anania, Phys. Rev. Lett. **43**, 1799 (1979).
[17] K. Matsuda, Y. Matsuda and G. E. Guest, General Atomic Report No. GA-A15351 (1979).
[18] V. Krapchev and A. Bers, Nucl. Fusion **18**, 519 (1978).
[19] R. W. Motley, S. Bernabei, W. M. Hooke and F. J. Paoloni, Nucl. Fusion **20**, 1207 (1980).